Biophysical Journal Volume 69 October 1995 1284–1298

A Cellular Automaton Model for the Proliferation of Migrating Contact-Inhibited Cells

Yih Lee, Stylianos Kouvroukoglou, Larry V. McIntire, and Kyriacos Zygourakis
Department of Chemical Engineering and Institute of Biosciences and Bioengineering, Rice University, Houston, Texas 77251-1892 USA

ABSTRACT A cellular automaton is used to develop a model describing the proliferation dynamics of populations of migrating, contact-inhibited cells. Simulations are carried out on two-dimensional networks of computational sites that are finite-state automata. The discrete model incorporates all the essential features of the cell locomotion and division processes, including the complicated dynamic phenomena occurring when cells collide. In addition, model parameters can be evaluated by using data from long-term tracking and analysis of cell locomotion. Simulation results are analyzed to determine how the competing processes of contact inhibition and cell migration affect the proliferation rates. The relation between cell density and contact inhibition is probed by following the temporal evolution of the population-average speed of locomotion. Our results show that the seeding cell density, the population-average speed of locomotion, and the spatial distribution of the seed cells are crucial parameters in determining the temporal evolution of cell proliferation rates. The model successfully predicts the effect of cell motility on the growth of isolated megacolonies of keratinocytes, and simulation results agree very well with experimental data. Model predictions also agree well with experimentally measured proliferation rates of bovine pulmonary artery endothelial cells (BPAE) cultured in the presence of a growth factor (bFGF) that up-regulates cell motility.

INTRODUCTION

Endothelial cells form a single layer that lines the entire vascular system. This thin monolayer regulates the exchange of nutrients and waste products between the bloodstream and the surrounding tissues. It also controls the transmigration of leukocytes from the bloodstream into adjoining tissues. Because almost all tissues need a blood supply, endothelial cells create an adaptable life-support system by pervading the blood vessels of every region of the body (Alberts et al., 1989; Thilo-Korner and Freshney, 1983).

Throughout the vascular system, endothelial cells retain a capacity for division and movement. Many studies (Grotendorst et al., 1981; Ross, 1993; Ross and Vogel, 1978) provide evidence that the response to endothelial injury may lead to thrombosis and abnormal smooth muscle proliferation as a result of the release of platelet-derived growth factor at sites where endothelial continuity is disrupted. Because both thrombosis and abnormal growth of smooth muscle cells are components of atherosclerosis lesion formation (Schwartz et al., 1980, 1981), endothelial growth is a necessary repair process for replacing cells lost through normal mechanisms of cell turnover. Several researchers have studied wound-associated regeneration in vivo (Haudenschild and Schwartz, 1979; Reidy and Schwartz, 1981; Schwartz et al., 1978, 1980) or in vitro (Klein-Soyer et al., 1986; Schwartz et al., 1980; Selden and Schwartz, 1979) by using mechanical methods to denude monolayers of endothelial cells. They found that if a wound is made in a cellular layer, neighboring cells migrate in and proliferate to cover the exposed surface.

The endothelial cells, like many normal mammalian cells, are anchorage dependent and require a substrate upon which they can spread and grow. Extracellular matrix plays a critical role in regulating cell shape, polarity, and growth (Ingber, 1990; Wang and Ingber, 1994). Growth of endothelial cells (unlike that of fibroblasts, smooth muscle cells, or other cells), however, is characterized by the formation of a highly ordered confluent monolayer in which neighboring cells touch one another. If during this process a cell becomes surrounded by other cells, it will stop growing. As a result of these contact-inhibition phenomena, only a fraction of the viable cells of a large population will continue to grow and divide after the initial stages of this process. This fraction decreases with increasing cell density and depends strongly on cell motility and on the initial conditions of the culture (seeding density and spatial distribution of inoculum) (Zygourakis et al., 1991a).

Substantial motility of endothelial cells has been observed under conditions (such as wound healing) that expose the cells to growth factors. Sato and Rifkin (1988) found that when a confluent monolayer of bovine aortic endothelial cells was wounded with a razor blade, the cells started to rapidly move from the edge of the wound into the denuded area. This migration was regulated by basic fibroblast growth factor (bFGF) released by the cells themselves. These results indicated that bFGF was responsible for the enhanced motility and the increased proliferation rates of the endothelial cells.

Similar enhancements of proliferation rates induced by increases in cell motility were observed and carefully characterized for another system. Barrandon and Green (1987) studied the growth of isolated megacolonies of coherent

Received for publication 30 August 1994 and in final form 22 June 1995.

Address reprint requests to Prof. Kyriacos Zygourakis, Department of Chemical Engineering, Rice University, MS 362, Houston, TX 77251-1892. Tel.: 713-527-8101, ext. 3509; Fax: 713-285-5478; E-mail: kyzy@rice.edu.

0006-3495/95/10/1284/15 $2.00

epidermal keratinocytes and found that both epidermal growth factor (EGF) and transforming growth factor α (TGF-α) significantly increased the cell proliferation rates. Using [^{14}C]thymidine pulse experiments, these investigators found that the growth of the megacolony depended on the outward migration of rapidly proliferating cells located in a thin rim close to the perimeter of the megacolony. They concluded that the effect of EGF and TGF-α in promoting cell growth depended on their ability to increase the rate of cell migration.

Therefore, the proliferation rates of anchorage-dependent, contact-inhibited cells are strongly affected by two competing processes: contact inhibition and cell migration. The opposing effects of these processes complicate the analysis of data obtained from large populations of cultured cells. Thus, the success of experimental studies aimed at assessing the effect of chemical stimuli (e.g., growth factors) on regulating the proliferation rates of cultured cells will depend on our ability to differentiate between the effects of (a) external factors (e.g., contact inhibition, density and spatial distribution of cells, surface geometry) and (b) changes in intracellular functions (e.g., mitogenic effects, up- or down-regulation of cell motility). The development of theoretical models that accurately describe the dynamics of populations of migrating cells during all stages of contact-inhibited proliferation can greatly facilitate the systematic analysis and evaluation of experimental data.

Some recent studies proposed models describing growth of populations of nonmotile cells. Frame and Hu (1988) developed a deterministic model in which the specific growth rate was expressed in terms of the cell density, even though in cultures of anchorage-dependent cells exhibiting contact inhibition only the cells at the perimeter of clusters can undergo division. Another model (Cherry and Papoutsakis, 1989) accounted for the importance of contact inhibition effects on the growth of nonmotile cells. Although the Cherry and Papoutsakis model assumed that the cell growth rate is proportional to the number of cells in the perimeter of a colony, it did not consider the merging of colonies. Furthermore, the assumption of circular cell colonies limited its applicability.

A stochastic model proposed by Lim and Davies (1990) relaxed the last assumption and took into account the topology of cell colonies. This model provided data not only on population dynamics but also on the patterns produced by clusters of cells in the colony. Ruaan et al. (1993) proposed another stochastic approach to model the growth of anchorage-dependent cells. This model considered cell movement within the first hour after division but made some restrictive assumptions that limit its usefulness for a detailed description of cell locomotion and cell-cell interactions.

Zygourakis et al. (1991a,b) developed a discrete model based on cellular automata (Tchuente, 1987) to describe the population dynamics of nonmotile contact-inhibited cells. This model captured the features of the proliferation process and included the important parameters (average cell size, seeding density, spatial distribution of cells) necessary for prediction of the properties of evolving cell populations. Forestell et al. (1992) and Hawboldt et al. (1994) also used cellular automata to model contact-inhibited cell growth on microcarriers. Cellular automata models have several advantages, including computational efficiency and the ability to describe in detail all the processes governing the growth of contact-inhibited cells.

This study reports the development of a more general cellular automata model that describes the proliferation of migrating contact-inhibited cells. Based on our experimental observations (Lee et al., 1994), the new model can accurately describe the persistent random walks executed by individual migrating cells, as well as the phenomena occurring when contact-inhibited cells collide with each other. Simulation and experimental results will be compared and analyzed to elucidate the competing roles played by contact inhibition and cell motility in determining proliferation rates.

DEVELOPMENT OF THE THEORETICAL MODEL

Locomotion of endothelial cells

Our experimental studies (Lee, 1994) on the locomotion of bovine pulmonary artery endothelial (BPAE) cells have shown that these cells execute persistent random walks in culture. Similar results were obtained earlier for microvessel endothelial cells by other investigators (Rupnick et al., 1988; Stokes and Lauffenburger, 1991; Stokes et al., 1991). After moving in a certain direction for some period of time, endothelial cells turn suddenly and migrate in a new direction. Direction changes occur either in response to some intracellular signal or because two cells collide. When two cells come close to each other, they slow down and one or both cells may lose the polarized (elongated) shape characteristic of migrating cells. Within 10–15 min after this event, however, both cells resume their polarized shapes with a leading lamella and move away from each other with increasing speed. When cells enter their mitotic phase, they slow down before they divide. After the division, both daughter cells execute persistent random walks with the same characteristics. As cell densities increase, contact inhibition starts to dominate and restricts the migration of the proliferating BPAE cells. Eventually, the BPAE cells stop migrating and proliferating and they form a compact, confluent monolayer.

A discrete model of these dynamic phenomena requires several parameters to describe the migration, interaction, and proliferation of contact-inhibited cells. A stochastic description of these processes based on Markov chain analysis is the most suitable approach (Noble and Levine, 1986) for obtaining the parameters of our discrete model.

Using a technique based on digital time-lapse recording and image processing (Lee et al., 1994), we monitored the migration of an entire population of BPAE cells during the first 2 days after seeding them on tissue culture plates. The cell trajectories were reconstructed (Lee, 1994), and we

found that we can approximate them with paths consisting of connected straight-line segments. Fig. 1 shows our approximations to some representative trajectories of BPAE cells for the time period of 12–48 h after seeding. Using a Markov chain analysis (Lee, 1994), we are able to measure (a) the local speeds of locomotion for individual cells; (b) the population-average speeds of locomotion; (c) the average waiting times for stationary and directional states (i.e., the average time a cell spends moving in a certain direction or remaining stationary); (d) the state-transition probabilities (i.e., the probabilities that a cell moving in a certain direction will turn and continue moving in another given direction); and (e) the steady-state probabilities (i.e., the probabilities that the cells will ultimately move in a certain direction).

Concept of cellular automata

Our simulations of cell migration and proliferation are carried out on cellular automata that are two-dimensional networks of computational sites. Each site is an automaton with a finite number of possible states that interacts with a finite number of neighboring sites. At discrete times, the computational sites change states, in parallel, by interacting with neighboring sites (Zygourakis and Markenscoff, 1991). Thus, cellular automata networks are discrete dynamical systems from the mathematical point of view. Such discrete systems provide an alternative approach to continuous models that use ordinary and partial differential equations to describe the dynamics of systems evolving in space and time.

Fig. 2 shows a confluent monolayer of BPAE cells. Clearly, BPAE cells at confluence may be represented by external irregular polygons with five or six sides. To construct a cellular array suitable for modeling BPAE cell migration and proliferation, we superimpose a uniform grid on the BPAE cell monolayer to define a lattice with square computational sites. A computational site that contains the nucleus of a cell is considered as occupied, otherwise it is designated as free. The use of a square lattice does not mean that the model assumes square living cells, an assumption that does not reflect the true morphology of migrating or confluent BPAE cells. Our earlier studies have shown (Zygourakis et al., 1991a,b), for example, that realistic cell colony patterns can be achieved with square lattices by assigning different "growth" probabilities to the neighbors of each computational site. The major advantage of square lattices is that they allow us to use data structures that minimize memory and computational time requirements.

As mentioned before, migrating BPAE cells execute persistent random walks with varying speed as they go through their division cycles (Lee, 1994). In addition, individual cells that are freely dividing in cultures have widely variable cycle times (Alberts et al., 1989). These random dynamic processes can be modeled on a cellular automaton by appropriately choosing the rules that govern the temporal evolution of the state of each computational site.

States of cellular automata

Our cellular automaton is a dynamic system evolving with discrete parallel iterations. At equally spaced time instants

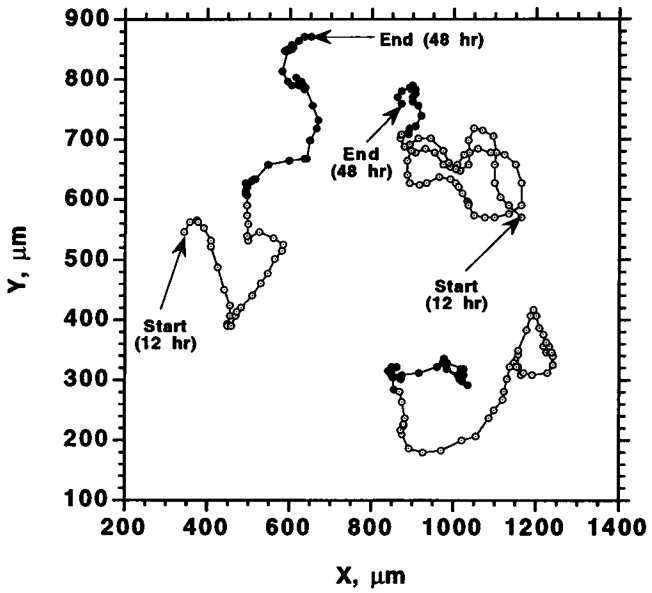

FIGURE 1 Typical trajectories of bovine pulmonary artery endothelial (BPAE) cells between 12 and 48 h after inoculation. The time interval between two successive symbols on a cell trajectory is 30 min. Open circles are used to denote the trajectories of parent cells, and solid circles show the trajectories of daughter cells. For simplicity, the trajectory of only one of the daughter cells is shown in each case.

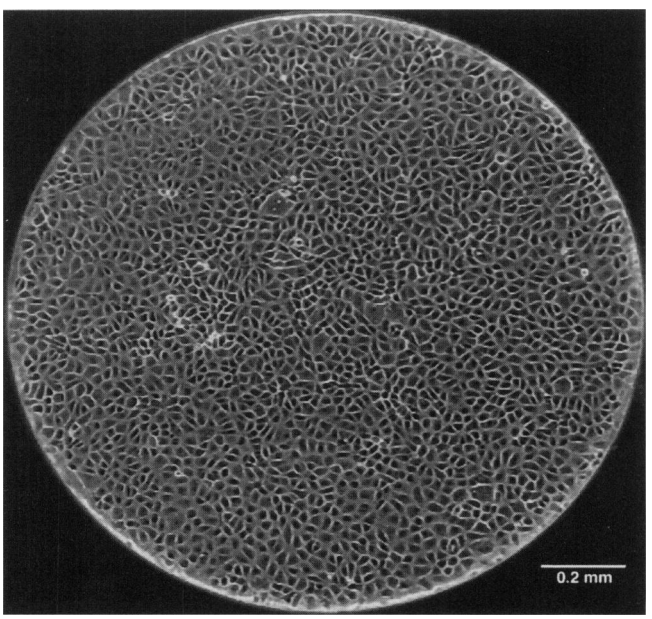

FIGURE 2 Digital image showing a confluent monolayer of BPAE cells in a well of the Terasaki microtest plate.

$t^1, t^2, \cdots, t^r, t^{r+1}, \cdots$ (where $t^{r+1} = t^r + \Delta t$ for all r), the state x_i of each automaton i ($i = 1, 2, \cdots, M \times N$, where M and N are the dimensions of the cellular array) evolves through interactions with neighboring sites. Each computational site is a multistate automaton that can either be occupied by a living cell, or be free and available for cell movement and division.

To simulate persistent random walks and asynchronous proliferation of cells in a two-dimensional cellular automaton, we must first define an appropriate set of values for the state x_i of each computational site. When a site contains a living cell, the state x_i of this automaton must specify (a) the direction in which this cell is moving, (b) the instantaneous speed of locomotion, (c) the time remaining until the next direction change, and (d) the time remaining until the next cell division.

In our model, cell migration occurs only in discrete steps, and a migrating cell will move into an adjacent free site within the time interval Δt. Since cells cover a fixed distance in every step, the average speed of the cell population can be varied by adjusting the time interval Δt of the parallel iterations. When a cell does not move at the average speed of the population, it remains at the same site (stationary state) for the current iteration. As we will see later, the adjustment of the transition probability for the stationary state gives us an additional means of regulating the speed of locomotion. With this simplification, the state x_i of an automaton i containing a migrating cell must only specify the direction of locomotion and the times remaining until the next direction change and the next cell division. Thus, the state x_i of an arbitrary automaton i takes values from the following set of 4-digit integer numbers

$$\Gamma = \{klmn | k,l,m, \text{ and } n \text{ are integers}\}$$

where k is the direction index. It denotes the direction in which the cell is currently moving. l is the persistence counter. The time t_c remaining until the next change in the direction of cell movement is equal to $t_c = l\ \Delta t$. mn is the two-digit cell phase counter. The time t_r remaining until the next cell division is equal to $t_r = (10m + n)\Delta t$.

Our model assumes that each computational site has eight nearest neighbors (Moore neighborhood) and that a migrating cell may move into any of the eight adjacent sites (if that site is free). Thus, the direction index k can take values from the set $\{0, 1, 2, \cdots, 8\}$ where the integers $1, 2, 3, \cdots, 8$ denote the directions of the eight neighbors in a counterclockwise order (1 = east direction, 2 = northeast direction, etc.). When a cell becomes stationary, its direction index takes the value of zero. The average waiting time computed by applying a Markov chain analysis (Noble and Levine, 1986) to the cell trajectory data provides the initial value of the persistence counter l after each direction change. At each iteration, the value of this counter is decremented by 1 and the cell changes direction when this counter reaches zero. Finally, the initial value of cell phase counter mn is randomly assigned to each living cell, using the cell division time distribution obtained from experiments. Again, the value of this counter is decremented by 1 at each iteration and the cell divides when this counter reaches zero.

Let us assume, for example, that simulations are carried out on a square lattice with $N \times N$ sites and that the time step is equal to $\Delta t = 0.5$ h. Furthermore, let the state of an arbitrary site i be equal to $x_i = 3319$ at some time t_0. This means that site i is occupied by a cell that is moving to the north. Migration in this direction will continue for three more time intervals (1.5 h), and the cell will divide after 19 iterations (9.5 h). At time $t_0 + \Delta t$, this cell will occupy the site $i + N$ located to the north of site i and $x_{i+N} = 3218$ (that is, the persistence and cell phase counters have been decremented by 1). If no other cell moves into the ith site, $x_i = 0$ at $t_0 + \Delta t$.

Algorithm for cell migration and proliferation

Each simulation starts by randomly distributing the seed cells to computational sites of the cellular automaton. The state of each occupied site is then set by randomly assigning a value to its direction index and setting the persistence and cell phase counters according to the experimental data. The rules governing the temporal evolution of the states of the automata are chosen to describe cell movement and division and are summarized below.

Algorithm

Initial condition. Using the specified cell seeding density and the spatial distribution of seed cells, select the sites that will be occupied by cells at time $t_0 = 0$. Specify the state of each occupied site by randomly selecting the direction index, by assigning the proper value to the persistence counter, and by setting the cell phase counter according to the experimentally determined distribution of cell division times.

At each time level $t^r = t^{r-1} + \Delta t$, $r = 1, 2, \cdots$

1. Randomly select an automaton (site).
2. If this automaton contains a cell and it is time for it to divide (that is, the cell phase counter is equal to zero), execute the division routine and go to step 5.
3. If this automaton contains a cell and it is time for a change in direction (that is, the persistence counter is equal to zero), execute the direction change routine and go to step 5.
4. Otherwise, try to move the cell to a neighboring site in the direction indicated by the direction index of its current state. If this site is free, mark it as the site that will contain the cell at the next time level and decrement the persistence and cell phase counters by 1. But if this site is occupied, the cell will remain at the present site and execute the direction change routine at the next iteration.
5. Select another automaton and repeat steps 2–4 until all automata have been examined.

6. Update the states of all automata to set the locations of all cells at the next time level.

Direction change routine. 1. Scan the neighborhood of the current site to determine if there are any free adjacent sites. If all sites are occupied, the cell remains at the present site.

2. If there are free sites in the neighborhood, select one of these sites according to a random algorithm based on the experimentally determined state-transition probabilities $p(i|j)$, $i,j = 0, 1, 2, \cdots, 8$.

3. Mark the selected site that will contain the cell at the next time level. Once a site has been marked in this fashion, no other cell can move in it at this iteration. Set the persistence counter to its appropriate initial value, decrement the cell phase counter, and return.

Division routine. 1. Scan the neighborhood of the current site to determine if there are any free adjacent sites. If all adjacent sites are occupied, the cell will not divide.

2. If there are free sites in the neighborhood, select one of these sites by using a random algorithm based on the growth probabilities (Zygourakis et al., 1991a).

3. Mark the selected site that will contain one of the daughter cells at the next time level. The second daughter cell will occupy the current location. Set the persistence and cell phase counters and return.

Note again that cells move in discrete steps from one site to a neighboring one, whereas the time step Δt corresponding to each iteration is variable. The size h of a square site is determined by the average size of the living cells. For the simulations discussed here, the square sites have a side equal to 28 μm, which makes them equal in area to the average BPAE cell at confluence. If $\Delta t = 0.5$ h, the instantaneous speed of a migrating cell is 56 μm/h if it moves in the east, north, west, or south directions. For $\Delta t = 1$ h, 2 h, $\cdots$, the instantaneous speeds of locomotion would be 28 μm/h, 14 μm/h, $\cdots$, respectively.

Our model can also compute the temporal evolution of the population-average speed of locomotion, which can be used to illustrate the effect of contact inhibition on populations of proliferating cells. After every iteration, we compute the sum of the distances (h or $\sqrt{2}h$, depending on the direction of motion) covered by all migrating cells. The population-average speed of locomotion at that particular time point is computed by dividing this sum by the total number of cells (migrating or not) and by the time interval Δt.

Estimation of model parameters from experimental data

The following is a summary of how the model parameters used for our simulations are estimated from experimental data obtained in our laboratory.

1. Area of a computational site: The area of each computational cell is set equal to the average size of the living cells at confluence. We have computed that, for BPAE cells at confluence, the average cell area is 617 μm^2 and the average area-equivalent radius is 14 μm (Lee et al., 1994).

2. Size of computational array: All of the simulations discussed here are carried out on computational grids containing either 1,513 or 61,517 computational cells. The smaller array is used to simulate cell growth in wells of Terasaki microtest plates. These wells are approximately 1.1 mm in diameter. The larger array is used to simulate cell culture in 96-well culture plates with 7-mm-diameter wells.

3. Seeding density and spatial location of the seed cells: The number of seed computational cells should match the given inoculum concentration. The spatial distribution of seed computational cells is determined by the experimental inoculation procedures.

4. Cell division time distribution: Using the computer-assisted analysis techniques described elsewhere (Lee et al., 1994), we measured the time elapsed between the first and second divisions of cultured BPAE cells after they were inoculated on the tissue culture plates. All of these measurements were performed during the time period from 12 to 48 h after inoculation. The measured distributions of cycle times for BPAE cells were used to set the initial value of the cell phase counter of each cell.

5. Speed of locomotion: The average speed of locomotion was computed from the cell trajectory data. If $d_j, j = 1, 2, \cdots, K$ are the lengths of the segments traveled by the jth cell between time levels t_{j-1} and $t_j = t_{j-1} + \Delta t$, the local speed of locomotion for this cell is given by

$$v_j = \frac{d_j}{\Delta t}$$

and the average speed for the cell over the time interval $[0, K\Delta t]$ is

$$\bar{v} = \frac{\sum_{j=1}^{K} d_j}{K(\Delta t)}$$

By averaging the speeds of all cells, the population-average speed of locomotion can be computed for each experiment and used in the simulations.

6. Average waiting time: Using a Markov chain approach (Noble and Levine, 1986), we computed the average time that a migrating cell spends moving in each of eight defined directions or in the stationary state.

7. State-transition probability: The state-transition probabilities $p(i|j)$ giving the likelihood that a cell in state j will jump to state i ($i,j = 0, 1, 2, \cdots, 8$) were also computed from Markov chain analysis (Noble and Levine, 1986). The model uses these probabilities to decide the new state of the cell (new direction of movement or stationary state) whenever the persistence counter reaches zero. Several studies have shown (Lee et al., 1994; Rupnick et al., 1988; Stokes and Lauffenburger, 1991; Stokes et al., 1991) that endothelial cells change their direction of locomotion in a gradual fashion with small angle changes. The transition probabilities for large angle changes are small.

Additional computer implementation details

The algorithm described above updates the state of all of the computational sites at each iteration. It is well known, however, that simulation results will exhibit computational artifacts if the sites are scanned in a fixed sequential order. For example, cell migration and proliferation will occur preferentially along directions coinciding with the fixed directions in which one scans the computational sites. To eliminate such artifacts, the sites must be scanned in a random order that changes from iteration to iteration. One approach would be to create a random ordering of all of the computational sites at the beginning of each iteration. For an $N \times N$ computational array, this random ordering would require N^2 calls to the random number generator function at each iteration.

To avoid the large overhead imposed by such a complete ordering of the sites, we only create random orderings of the N rows and the N columns at each iteration. We then scan the sites by rows according to the random ordering of rows. Within each row, scanning proceeds according to the computed random ordering of columns. New random orderings of the rows and columns are computed for each iteration. This approach requires only $2N$ calls to the random number generator function and reduces the computational time by more than 2 orders of magnitude. There were no differences between results from simulations carried out with complete and partial (row/column) orderings of the computational sites.

CPU times for typical runs with automata having 61,517 sites ranged from approximately 50 to 200 s on an IBM RS/6000 POWERStation 350 computer. For these runs, cells were seeded uniformly on a flat surface and the simulations continued until 100% surface coverage (confluence) was obtained in each case. As expected, CPU times show a strong dependence on the size of the computational array and the seeding density of the cells, because the latter parameter determines the number of iterations required to reach confluence. The CPU times also depend on the initial spatial distribution of the seed cells.

When cells are uniformly distributed with a fixed initial density on the computational grid, different seed numbers produce different sequences of random numbers and, therefore, different realizations of the initial condition for our simulations. Results from simulations with different initial realizations were nearly identical. This was due both to the large size of our grids and to the motility of the cells. Both of these factors minimize the importance of "edge" effects that are the main cause of differences among results from simulations with different initial realizations.

RESULTS AND DISCUSSION

We first present results from simulations carried out on computational grids with 61,517 sites. These runs simulate cell movement and growth on one well of the 96-well plates. Fig. 3 shows the three types of initial spatial distributions of seed cells used in the simulations presented in the following sections:

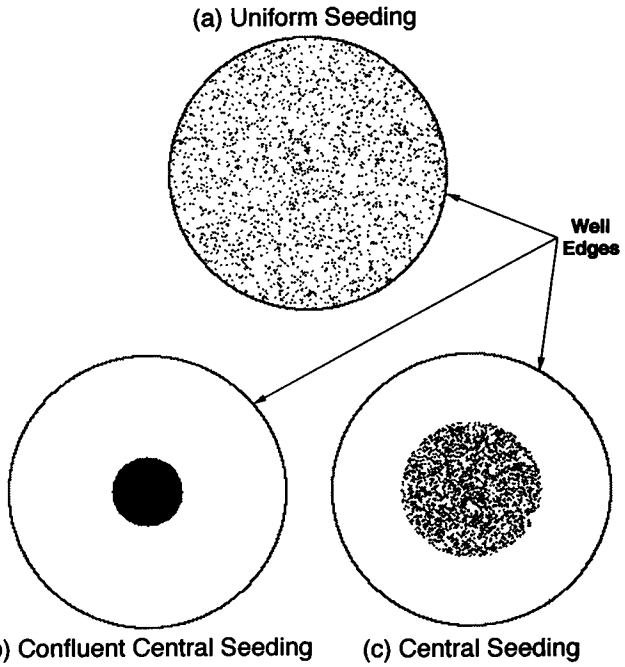

FIGURE 3 Seeding modes for simulations modeling migration, and proliferation of cells in 96-well plates. The grid for each well has 61,517 computational sites. All three initial configurations shown here have 3,853 cells seeded on grids with 61,517 sites (seeding density of 6.26%). Properties of BPAE cells are used to generate these grids. (*a*) Uniform seeding. Simulations start by distributing the seed cells randomly on the computational sites. (*b*) Confluent central seeding. Seed cells are placed in a confluent circular spot in the middle of the well. (*c*) Central seeding. Seed cells are randomly distributed in a high-density circular spot.

(a) uniform seeding with cells randomly distributed throughout the circular area available for cell growth;

(b) confluent central seeding with cells forming a confluent circular spot in the middle of the area available for cell growth; and

(c) central seeding with cells distributed randomly in a high-density circular spot.

For simplicity, the following approximation to the distribution of cell division times presented in the literature (Zygourakis et al., 1991a) was adopted for these simulations: 64% of the living cells have division times between 12 and 18 h, 32% of the cells have division times between 18 and 24 h, and 4% of the cells have division times between 24 and 30 h. The simulation results presented below will establish the relative importance of various experimental parameters and show how the proliferation rates of migrating cells are affected by contact inhibition and speed of locomotion.

Contact inhibition decreases the proliferation rates of nonmotile cells

Fig. 4 shows the effect of seeding density on the proliferation rate. The cells here are nonmotile and are uni-

formly seeded on the computational grids (see pattern of Fig. 3 *a*). For very low seeding densities (e.g., 0.33% or 1.63%), the surface coverage curves have a long "induction" period because the slow growth of isolated colonies dominates the process after the first few divisions. This induction period disappears as the seeding density increases above 3.25%. At higher seeding densities, the surface coverage increases rapidly as the cells reach confluence within a few divisions and before isolated cell colonies can form. The time required to reach confluence decreases with increasing seeding density. These results agree well with the data of Zygourakis et al. (1991a).

The adverse effects of contact inhibition can be better seen by observing sequences of computational grids obtained at different time levels. Fig. 5 (*a–c*) presents such a sequence of computational grids from a simulation with nonmotile cells. The seeding density for this run is 0.32%, and the initial configuration of the cellular array is shown in Fig. 5 *a*. After 3.5 days, we observe the formation of isolated colonies (Fig. 5 *b*) as the population reaches a surface coverage of 6.6%. After this point, contact inhibition dominates the cell proliferation process. Only cells located at the perimeter of isolated colonies can now divide and the relative number of proliferating cells decreases with each division (Zygourakis et al., 1991a,b). Mergings of cell colonies lead to additional reductions in the number of proliferating cells and further enhance the adverse effects of contact inhibition. At 7 days after inoculation, the population has only reached 36.1% surface coverage (Fig. 5 *c*).

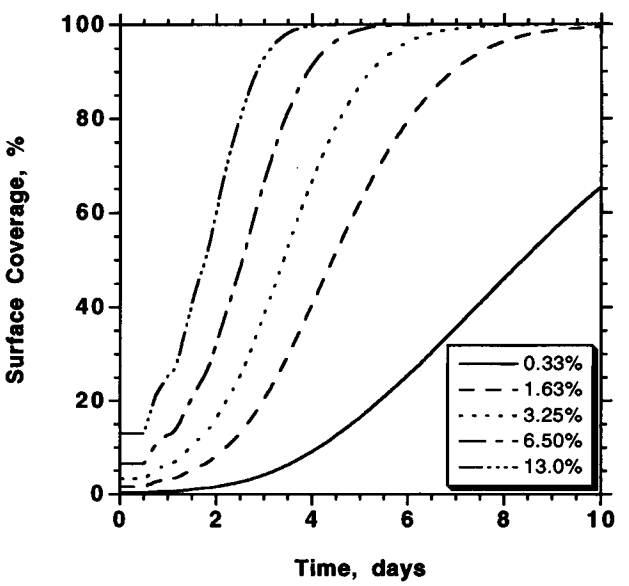

FIGURE 4 Effect of seeding density on the proliferation rate. All cells are nonmotile and are uniformly seeded. Properties of BPAE cells are used for these simulations.

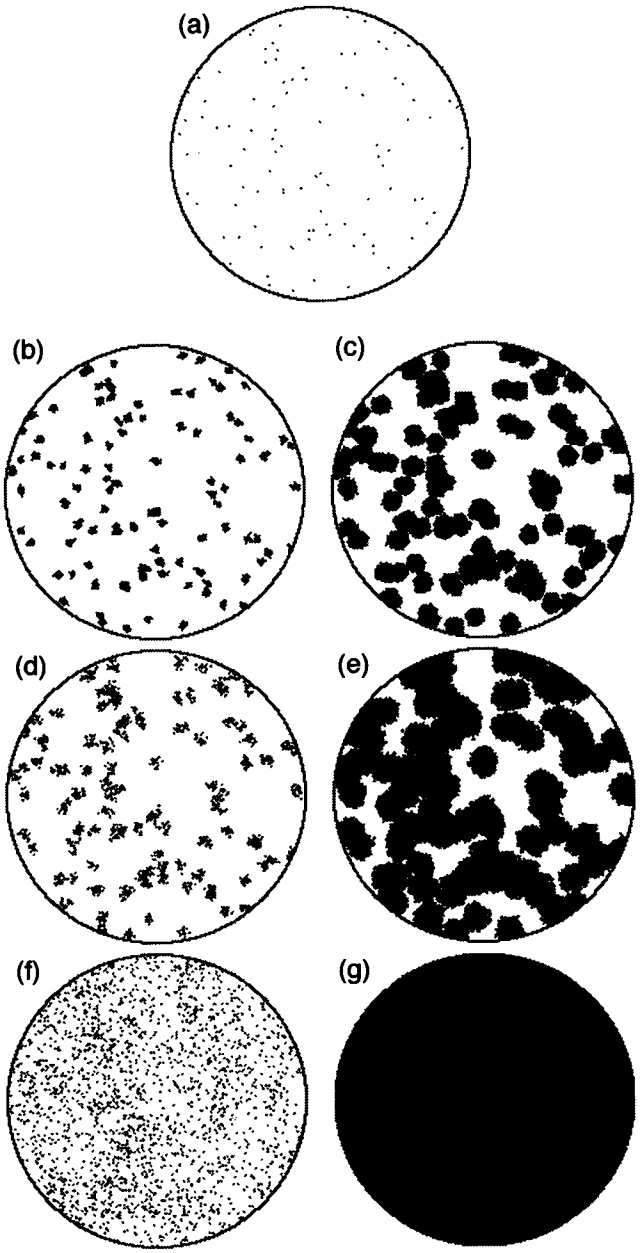

FIGURE 5 Predicted effect of cell motility on the spatial distribution of BPAE cells at different time levels. All three runs shown here start with the same initial configuration (*a*) and a seeding density of 0.32%. The computational sites occupied by cells are shown as black. (*b* and *c*) Spatial distribution of nonmotile BPAE cells 3.5 and 7 days after inoculation. (*d* and *e*) Spatial distribution of motile BPAE cells 3.5 and 7 days after inoculation. These cells migrate with an initial speed of locomotion equal to 1.75 μm/h. (*f* and *g*) Spatial distribution of highly motile BPAE cells 3.5 and 7 days after inoculation. These cells migrate with an initial speed of locomotion equal to 56 μm/h.

Motility reduces the adverse effects of contact inhibition on cell proliferation rates

The model predicts that motile contact-inhibited cells will proliferate faster than nonmotile cells with the same distribution of cell division cycle. This is because motile cells

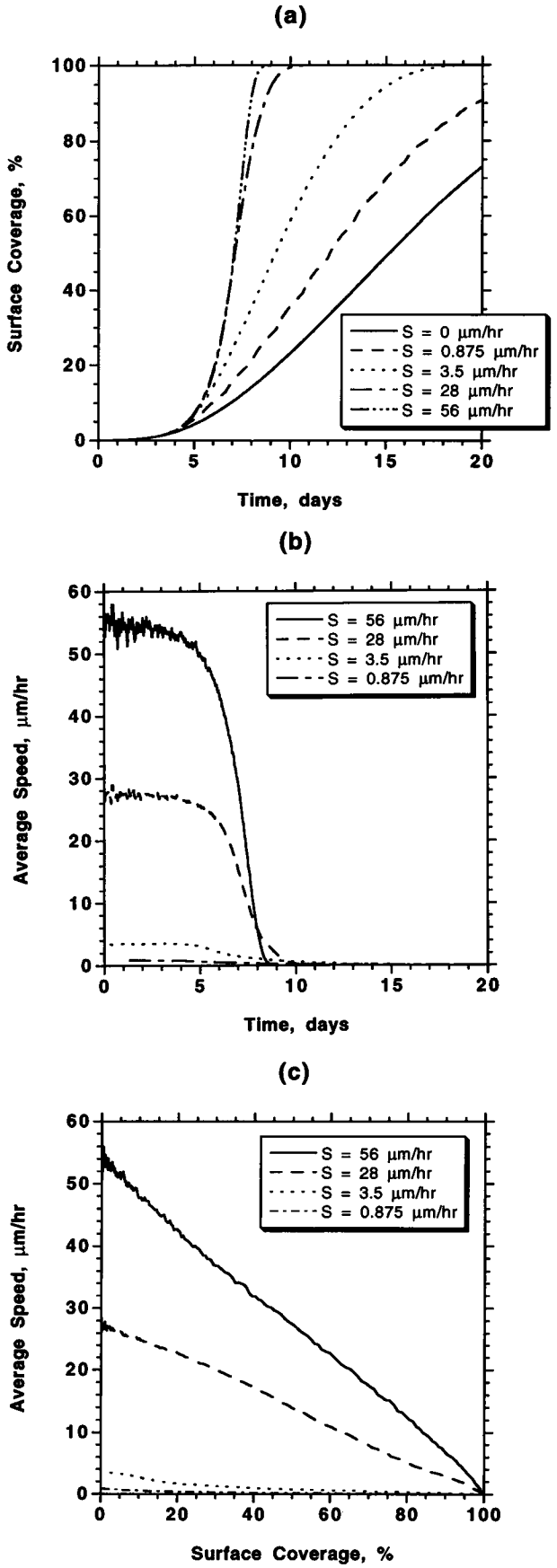

will move away from their neighbors, creating more space for all cells to continue migrating and dividing. Fig. 5 (*a, d,* and *e*) shows the computational grids from a simulation with motile cells migrating at an average speed of 1.75 μm/h. This speed of locomotion is very low for stimulated or unstimulated BPAE cells. Note that this run used the same initial configuration of seed cells as the previously discussed simulation with nonmotile cells (sequence of Fig. 5, *a–c*).

After 3.5 days from the start of the experiment, the simulation with motile cells shows the formation of rather "diffuse" cell colonies (Fig. 5 *d*) instead of the tightly packed colonies observed with nonmotile cells at the same time point (Fig. 5 *b*). Proliferation in the interior of these diffuse colonies continues because migrating cells move away from their neighbors, allowing them to divide and decreasing the adverse effects of contact inhibition on proliferation. After several more divisions, however, we again observe the formation of tightly packed cell colonies (see Fig. 5 *e*, showing the grid at the 7-day point), and contact inhibition effects start to dominate. We should note here that the cell colonies are much larger, indicating a later onset of severe contact inhibition. Also, the colonies exhibit a wide rim of migrating and proliferating cells, indicating that a sizable fraction of the cell population continues to divide.

Further increases in cell motility lead to further reductions in the importance of contact inhibition effects. Fig. 5 (*a, f,* and *g*) shows the computational grids from a simulation with motile cells migrating at an average speed of 56 μm/h, a high limit for the speeds we measured experimentally for stimulated BPAE cells. Note again that this run used the same initial configuration of seed cells as the previously discussed simulations with nonmotile cells (sequence of Fig. 5 *a–c*) and cells exhibiting low motility (sequence of Fig. 5 *a, d,* and *e*).

The high motility of cells in the last run completely compensates for the adverse effects of contact inhibition. The computational grid at 3.5 days shows no indication of colony formation, and cells appear to be uniformly distributed on the culture area (see Fig. 5 *f*). After a few more divisions, the cell density increases dramatically, and almost complete confluence is reached 7 days after inoculation (Fig. 5 *g*). Contact inhibition does not become significant until the final stages of growth, and the time required to obtain complete coverage of the surface is not significantly delayed.

It is important to emphasize again that all three simulations discussed here start with the same initial configuration

FIGURE 6 (*a*) Model predictions showing the effect of the population-average speed of locomotion S on cell proliferation rates. (*b*) Temporal evolution of the population-average speed of locomotion for cell populations with different motile activities. (*c*) Dependence of population-average speed of locomotion on cell density. The uniform seeding mode, the properties of BPAE cells, and an initial cell density equal to 0.081% were used for these simulation runs.

and show a 6.6% surface coverage after 3.5 days. However, the spatial distributions of cells at this time point are different for the three simulations (compare Fig. 5 *b, d,* and *f*), and severe contact inhibition effects slow the growth of populations with nonmotile or low-motility cells. At day 7 after inoculation, the surface coverage values are 36.1%, 60.3%, and 99.7%, respectively, for the runs with nonmotile, low-motility, and high-motility cells.

The growth curves shown in Fig. 6 *a* further demonstrate the effects of motility on cell proliferation. All of these runs start with a low seeding density equal to 0.081%. At first, small increases in motility (see curves for average speeds of 0.875 and 3.5 μm/h) have a dramatic effect on cell proliferation, and the times required to reach confluence decrease rapidly with increasing cell motility. The incremental enhancement of proliferation rates, however, diminishes as the average speed of locomotion reaches values above 5 or 10 μm/h for such simulations.

Fig. 6 *b* shows the temporal evolution of the population-average speed of locomotion. The average speed of locomotion remains fairly constant for the first few days, when cell densities are relatively low (flat initial portion of the growth curves of Fig. 6 *a*). As the cell densities increase further, however, the average speed decreases rapidly with time. Large cell densities lead to an increase in the number of cell-cell collisions, which drive the average migration speed of the population to lower levels. The strong dependence of locomotion speed on cell density is shown in Fig. 6 *c*, where the average speed is plotted versus surface coverage. An almost linear relation between average speed and cell density is indicated by this figure.

When the initial seeding densities increase, the beneficial effects of motility on the cell growth curves diminish. Fig. 7 presents simulation results from runs with 0.81% seeding cell density. The curves show smaller growth rate enhancements due to cell motility than those we observed in runs with the lower seeding density of 0.081% (Fig. 6 *a*). These observations have significant implications for the design of experiments aimed at studying the role of cell motility on proliferation.

The persistence of cell random walks affects the proliferation rates only slightly

We have also investigated how the average waiting time between direction changes of migrating cells (i.e., the persistence of their random walks) affects their proliferation rates. Simulation results showed a minimal effect of the average waiting time on the proliferation rate of highly motile cells that were uniformly seeded at low initial densities. The simulations also revealed that short waiting times (low persistence) slow down the rate at which the average speed decreases with increasing surface coverage. Long waiting times (high persistence) increase the likelihood of cell-cell collisions, and the average locomotion speed of the population decreases faster with increasing cell density.

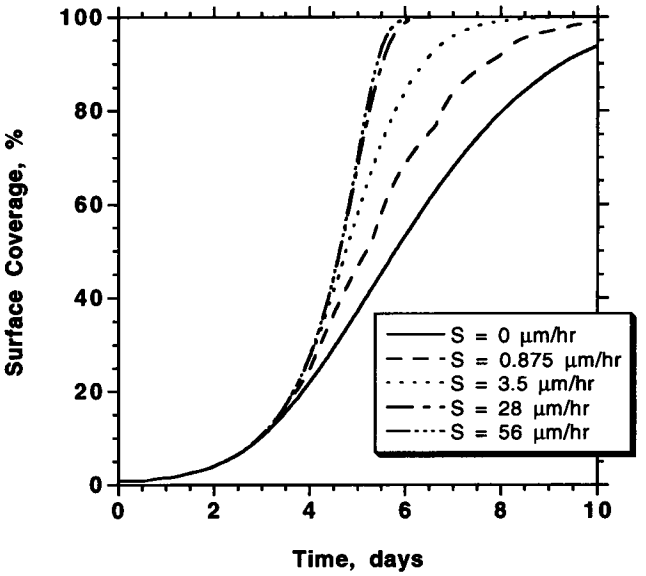

FIGURE 7 Model predictions showing the effect of speed of locomotion S on cell proliferation. The uniform seeding mode, the properties of BPAE cells, and an initial cell density equal to 0.81% were used for these simulation runs.

Growth of megacolonies

All of the simulations discussed in the previous sections started by distributing the seed cells uniformly and randomly on the computational grid (see seeding mode of Fig. 3 *a*). Several studies have shown, however, that the uniform seeding mode is not a good model for quantifying the wound healing response of endothelium (Gotlieb et al., 1984; Klein-Soyer et al., 1986; McNeil et al., 1989; Sato and Rifkin, 1988). Several other investigators also used different seeding modes to analyze the effects of cell motility on proliferation.

Barrandon and Green (1987) studied the growth of isolated megacolonies of coherent epidermal keratinocytes cultured with and without growth factors. Each megacolony was grown from a single cell that was isolated from an 8-day-old clone and reinoculated into a separate dish containing lethally irradiated 3T3 cells to support multiplication. Results from this study showed large increases in the growth rates of megacolonies when EGF or TGF-α was added to the culture media. Through a careful analysis of their data, Barrandon and Green determined that the growth rate of a megacolony depended on the outward migration of the rapidly proliferating cells located in a thin rim close to the colony perimeter. They concluded that the growth factors should not be viewed as simple mitogens and that their effectiveness in promoting cell proliferation must depend on their ability to up-regulate cell migration.

We will now use the confluent central seeding mode shown in Fig. 3 *b* as the initial condition for simulations aimed at studying the effect of cell motility on the growth of megacolonies. Simulations start by placing the seed cells in a confluent circular spot or megacolony located in the center

of the growth surface. Fig. 8 (*a–d*) presents four sequences of images showing the computational grids at three different time levels for runs with cells migrating at speeds of 0, 14, 28, and 56 μm/h, respectively. Every sequence shows the grids at 2 days (top panel), 4 days (middle panel), and 6 days (bottom panel) after the start of the simulation. The gray area in the center of these images denotes the initial megacolony, and the black area at the perimeter shows the relative growth of the megacolony at the various time points.

A megacolony of nonmotile cells (sequence of Fig. 8 *a*) expands very slowly because only the cells at the perimeter can grow at the normal rate. When cells become motile (by adding, for example, a growth factor to the culture medium), the size of the colony increases at much faster rates (see sequences in Fig. 8, *b–d*). Motile cells migrate in an outward direction and form a pronounced "proliferation rim." Cell densities decrease as we move in an outwardly radial direction in this rim, as cells move away from their neighbors, diminishing the effects of contact inhibition. As shown by the sequences of Fig. 8, the thickness of the proliferation rim increases rapidly with increasing speeds of locomotion. For highly motile cells (Fig. 8 *d*), the megacolony quickly reaches the edge of the culture area, in contrast to the very slow growth of the megacolony of nonmotile cells shown in Fig. 8 *a*.

Fig. 9 summarizes the effect of speed of locomotion on megacolony growth measured by the normalized radius $R(t)/R_0$, where R_0 is the initial radius of the confluent megacolony and $R(t)$ is the radius of the megacolony at some subsequent time t. The initial slopes of these curves indicate that the normalized radii increase at constant rates. For megacolonies of cells moving with speeds equal to 0, 14, 28, and 56 μm/h, the ratio of expansion rates is 1:4.56:8.08:17.41. These results show an almost constant effect of cell motility on the colony growth rate, even for highly motile cells.

Simulation results also revealed a significant increase in the growth rates, with increasing average waiting time. The cells in the interior of the colony force the cells at the perimeter of the megacolony to move in an outward direction. Therefore, cells with longer average waiting times cover longer distances as they move away from the megacolony, thus increasing the width of the proliferation rim. On the other hand, cells with shorter average waiting times may move out and then bounce back, colliding with other cells and slowing the growth of the proliferation rim.

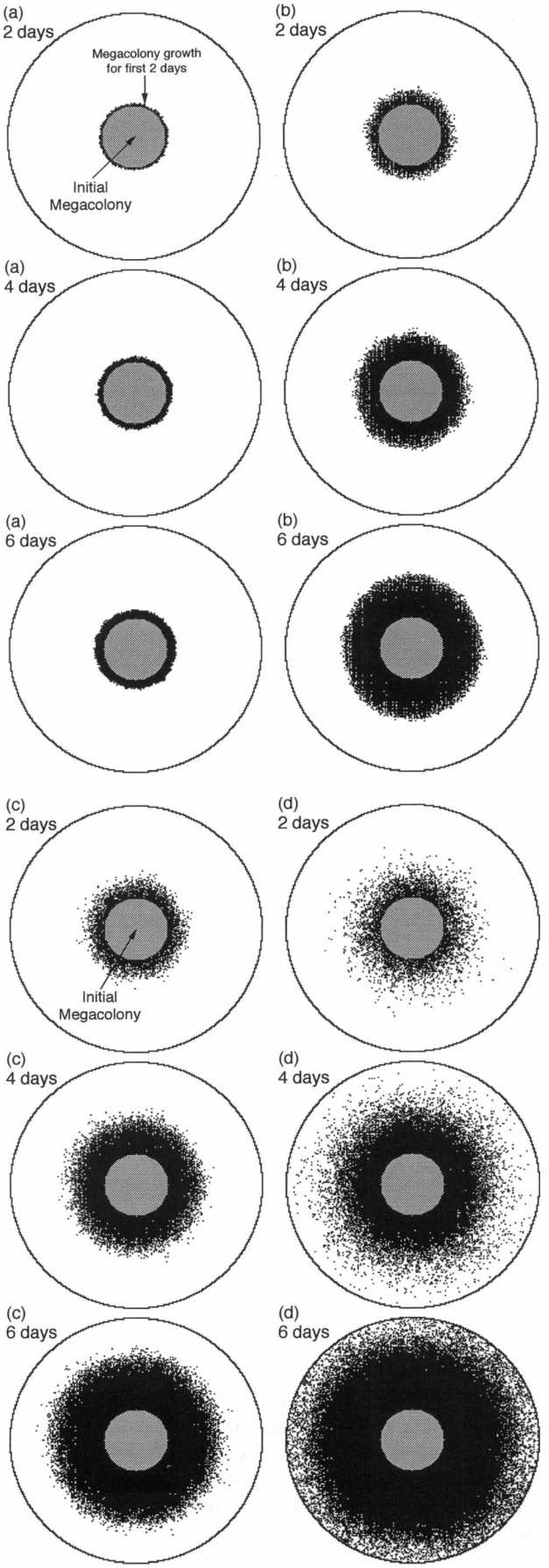

FIGURE 8 Four sequences of images showing the predicted growth of megacolonies of cells with different motilities. Every sequence shows the computational grid at 2, 4, and 6 days (top, center, and bottom) after inoculation. The computational sites occupied by cells are shown as black. The properties of epidermal keratinocytes and an initial cell density of 6.26% were used for these simulation runs. Sequence a: Growth of a megacolony of nonmotile cells. Sequence b: Growth of a megacolony of motile cells with $S = 14$ μm/h. Sequence c: Growth of a megacolony of motile cells with $S = 28$ μm/h. Sequence d: Growth of a megacolony of motile cells with $S = 56$ μm/h.

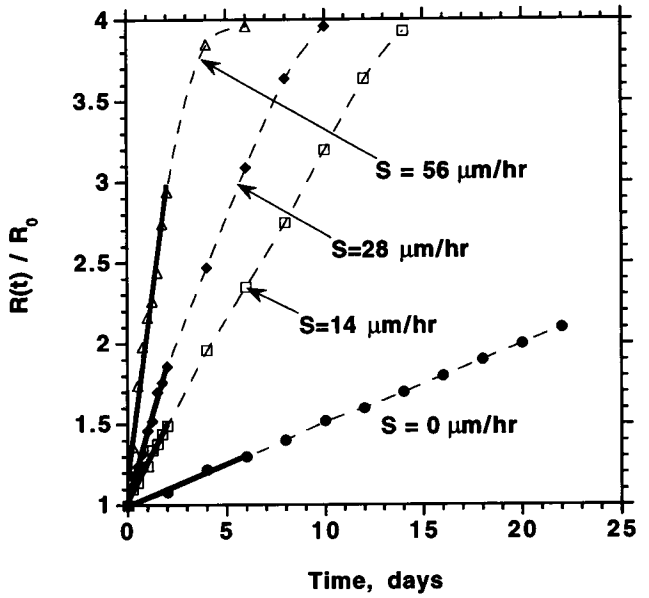

FIGURE 9 Model predictions showing the effect of speed of locomotion, S, on megacolony growth estimated by computing the normalized radius $R(t)/R_0$. ●, nonmotile cells; □, cells migrating with an initial speed of 14 μm/hr, ♦ cells migrating with an initial speed of 28 μm/h; △, cells migrating with an initial speed of 56 μm/h. The initial slopes (bold lines) indicate that the normalized radii increase at constant rates.

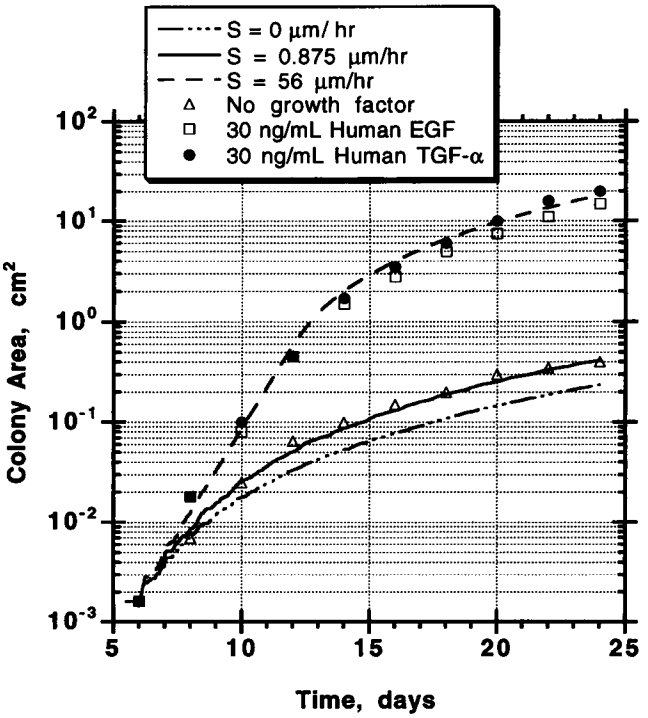

FIGURE 10 Comparison of model predictions and experimental data on the growth of isolated colonies of keratinocytes cultured with and without growth factors. Symbols: experimental data from Barrandon and Green (1987). Lines: Predictions from our cellular automata model.

To check the predictive capabilities of our model, we carried out simulations on large computational grids to study the growth of isolated megacolonies under the conditions employed in the experiments of Barrandon and Green. Because the speed of cell locomotion was not directly measured in that study, values for this model parameter were estimated from the experimental measurements of both the width and the rate of outward movement of the proliferation rim presented by Barrandon and Greene. Fig. 10 compares predictions from our cellular automata simulations to the experimental data of Barrandon and Green. The agreement is very good. Fig. 10 not only illustrates the strong dependence of proliferation rates on cell motility for certain cellular systems; it also shows the capability of our cellular automaton to accurately describe the dynamics of a proliferating cell population.

Heterogeneities in the spatial distribution of seed cells

We are also interested in investigating how heterogeneities in the spatial distribution of seed cells may affect the observed cell proliferation rates. Spatial heterogeneities are common (albeit undesirable) consequences of inoculation and culture protocols. One simple model of spatially heterogeneous inocula is the central seeding mode shown in Fig. 3 *c*, where the seed cells are distributed at high density in a circular spot located in the middle of the culture area. Clearly, this is an "intermediate" case between the uniform and the confluent central seeding modes shown in Fig. 3 *a* and *b*. For the seeding mode of Fig. 3 *c*, cells are seeded in a circle covering 25% of the total circular culture area.

Fig. 11 compares the effects of speed of locomotion on the proliferation rates for confluent central (thin lines) and central seeding modes (thick lines). If the cells are nonmotile, the growth curve for the population starting with central seeding (bold solid line) shows a biphasic behavior. Initially, it coincides with the growth curve of motile cells that have the same seeding distribution. Because of the high density, however, confluence is quickly reached in the central spot and the surface coverage reaches 25% (the size of the central spot) within a few cell divisions (2.5 days). After reaching this point, the growth rate decreases significantly as cell proliferation becomes severely contact inhibited and the megacolony grows at the very low rates exhibited by nonmotile cells (see Figs. 8 and 9).

Fig. 11 also shows significant differences in the growth curves of motile cells seeded with the two patterns of Fig. 3 *b* and *c*. These results clearly imply that spatial heterogeneities in the seeding distribution can have significant effects on the observed growth rates, even for highly motile cells.

Cell growth on the surface of three-dimensional objects

All of the simulations presented above model cell migration and proliferation on flat domains corresponding to the bot-

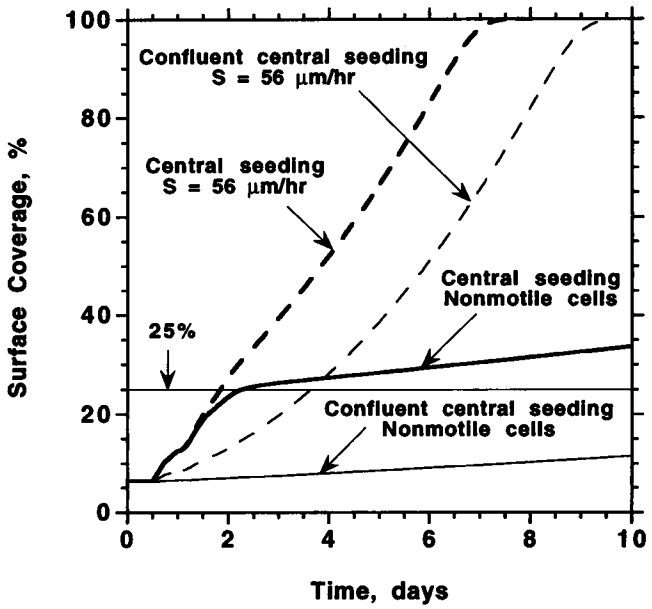

FIGURE 11 Model predictions showing how inhomogeneities in the initial spatial distribution of cells can affect the proliferation rates of motile (dashed lines) and nonmotile BPAE cells (solid lines). The confluent central and the central seeding modes (thin and thick lines, respectively) were used for these simulations with an initial cell density of 6.26%.

tom of circular wells. Our model, however, can easily handle cell growth on the surface of some simple three-dimensional objects by imposing periodic boundary conditions at the edges of the growth surfaces. We have used this approach to model cell migration and proliferation on the surface of (a) cylindrical tubes and (b) tori. Results from such simulations can be applied to study cell locomotion and growth on the surfaces of hollow-fiber capillaries and spherical microcarriers.

Our simulation results show that if enough cells are seeded on a surface, the geometry of the growth surface does not significantly affect the proliferation rates of motile or even nonmotile cells. Surface geometry effects become important only at extremely low seeding densities. Small differences of proliferation rates are observed for nonmotile cells at low densities because of edge effects (Zygourakis et al., 1991a). For motile cells, however, the importance of edge effects diminishes.

Model predictions agree with experimental proliferation data for BPAE cells

In this section we will compare model predictions to experimental data obtained in our laboratory with bovine pulmonary artery endothelial cells. Details of cell culture have been given in an earlier publication (Lee et al., 1994). The locomotory parameters for the cellular automata model were obtained by using the microscope-stage incubator and the digital time-lapse technique described in the same publication. To obtain motility data for each experiment, an average of 50 cell paths were reconstructed for the time period from 12 to 48 h after incubation. Our experimental results showed that bFGF significantly enhanced cell motility. When bFGF was added to the culture media at a concentration of 30 ng/ml, the average speed of locomotion increased from 0.4 μm/min (24 μm/h) for no bFGF to about 0.7 μm/min (42 μm/h) for 30 ng/ml bFGF. The addition of bFGF did not affect the average waiting time for the eight directional states, which was approximately equal to 0.7 h in all cases. However, the average waiting time of the stationary state decreased from 2.1 h to about 1 h when the cells were cultured with 30 ng/ml bFGF.

We analyzed these data further to compute values for all of the parameters of our cellular automata model. The addition of bFGF did not significantly affect the computed state-transition probabilities. In the absence of bFGF, the ratios of probabilities that a cell would make a 180°, 135°, 90°, or 45° turn were equal to 1:0.77:2.04:9.73, indicating that cells move with small-angle turns. The probability that a cell will make a ±45° turn was about an order of magnitude larger than the probability that it would make a 180° turn. When 30 ng/ml of bFGF was added to the culture medium, these probability ratios changed only slightly to 1:0.94:2.44:8.31.

We also measured the distribution of cell division times using the data from cell tracking experiments. From the 36-h time-lapse recordings, we identified the cells that divided more than once and measured the time that elapsed from the first division until the next division of the daughter cells. These distributions showed a shift to shorter division times in the presence of bFGF, indicating the mitogenic effects of bFGF on the growth of BPAE cells. The computed distribution of cell division times was used for the cellular automata simulations, as described earlier in the model development section.

An additional issue involving the initial conditions for our simulations must be discussed before we can compare model predictions to experimental data. As is common with endothelial cell cultures, the experimental cell counts did not change appreciably in the time interval between 12 and 24 h after inoculation. During this initial period, the BPAE cells adhere to the tissue culture surface, spread, and start migrating. We observed, however, that the period between inoculation and the first division varied widely among the cells of a population. Whereas some cells divided during the period between 12 and 18 h after inoculation, other cells required more than 24 h for their first division. The wide variability of this initial spreading time complicates the choice of the initial conditions for our simulations. For the first division of the cells, the cell phase counters must be loaded with a distribution of division times that also includes the period required for spreading. If this is not done, the model will underestimate the time interval required for the first division of each cell and will overpredict the cell population in the initial stages of proliferation. Because model predictions are sensitive to the initial seeding density,

small errors in the predicted cell population in the initial stages will be magnified after several cell divisions.

Because the distribution of the duration of this initial period of cell spreading was not measured experimentally, a model parameter was employed to handle the highly asynchronous cell population resulting from our inoculation procedure. Every time the division routine was called, a random number was computed and compared to a division probability to determine if that cell would indeed divide. If that check gave a negative result, the cell continued to migrate while its cell phase counter remained at zero. Thus, the division routine would be called again at the next iteration and the process would be repeated until the cell divided. By delaying cell divisions in this fashion, we were able to simulate the effect of spreading times on cell proliferation.

Model predictions were compared to experimental cell counts from an independent set of proliferation experiments that were carried out to measure the growth rates of uniformly seeded cells in the wells of Terasaki plates. Every data point represented the average of three cell counts obtained from different wells of a Terasaki plate. Duplicate experiments were carried out for each set of conditions.

Fig. 12 shows the comparison between experimental cell counts and theoretical predictions for three different seeding densities of uniformly seeded cells cultured without bFGF. The simulation results agreed very well with the experimental data, which verified the predicted effect of cell seeding densities on proliferation rates and on the time required to achieve confluence.

Fig. 13 compares the normalized cell counts $N(t)/N_0$ from experiments and simulations for uniformly seeded cells

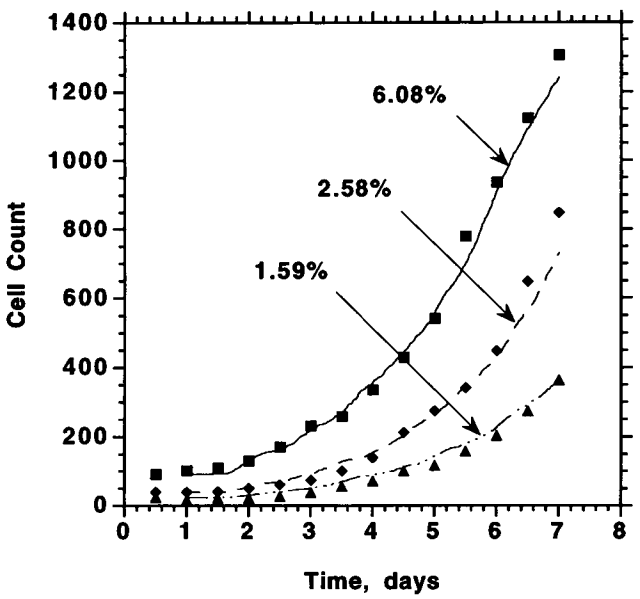

FIGURE 12 Comparison of experimental cell counts and theoretical predictions for BPAE cells cultured without bFGF. The cells were uniformly seeded at three different initial densities (1.59%, 2.58%, and 6.08%). The lag time is 24 h.

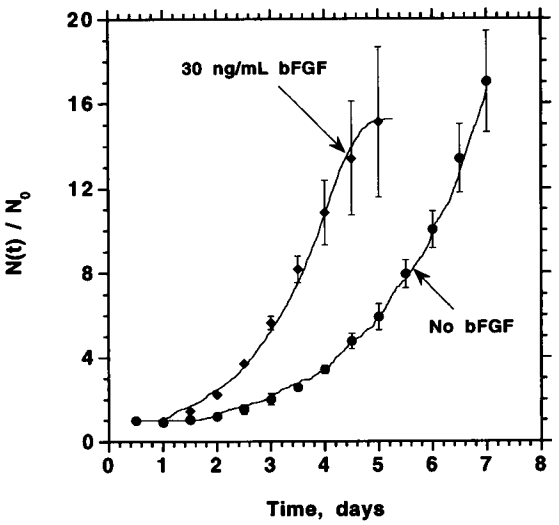

FIGURE 13 Normalized cell counts, $N(t)/N_0$, from experiments (symbols) and simulations (lines) for uniformly seeded BPAE cells cultured without and with 30 ng/ml bFGF. Standard errors are used as error bars. The lag times for simulations of no bFGF and 30 ng/ml bFGF are 24 and 12 h, respectively.

cultured without and with 30 ng/ml bFGF. The normalized cell counts are computed by dividing the cell count $N(t)$ at any time t by the cell count N_0 computed (or measured) at 12 h after inoculation. The final normalized cell counts were different for these two experiments because of variations in the actual sizes of the Terasaki plate wells. Our model again did an excellent job in fitting experimental data. These results confirm the mitogenic effects of bFGF and support the hypothesis that the proliferation rates of contact-inhibited cells depend on their speed of locomotion. The division probabilities were 0.02 and 0.04 for the runs simulating growth without bFGF and with 30 ng/ml bFGF, respectively. We must emphasize again that the division probability parameter can be eliminated if the distribution of spreading times is known for every set of conditions. However, such data are not yet available.

CONCLUSIONS

We have developed a comprehensive model that uses a cellular automaton to study the population dynamics of migrating and proliferating contact-inhibited cells. The discrete modeling approach was powerful enough to incorporate all of the essential features of the cell locomotion and division processes, including the complicated dynamic phenomena occurring when cells collide. But the model was also computationally efficient and will enable us to investigate the dynamics of cell populations significantly larger than the ones considered in this study.

The simulation results allowed us to evaluate the opposing effects of cell motility and contact inhibition on proliferation rates. Contact inhibition reduces the number of cells that can grow at the normal rate. By promoting wider

separation of the cells, on the other hand, high cell motility delays the onset of contact inhibition and enhances the proliferation rates. The relation between cell density and contact inhibition was studied by following the temporal evolution of the population-average speed of locomotion. We also investigated the influence of several system parameters on the proliferation rates. The seeding cell density, the population-average speed of locomotion, and the spatial distribution of the seed cells were found to be crucial parameters in determining the temporal evolution of cell proliferation rates.

These results have significant implications for the design of experiments. For example, we often probe intracellular functions and mechanisms by measuring how large cell populations respond to external stimuli like growth factors. For this approach to be successful, however, the possibly strong effects of contact inhibition must be "filtered" out from the experimental data. In addition to providing a systematic way for analyzing such data, the model presented here can be used to select appropriate experimental conditions. For example, our simulation results indicate that experiments designed to study the effects of cell motility on proliferation should use low seeding cell densities or central seeding patterns.

The model was successful in assessing the effect of cell motility on the growth of isolated megacolonies, and its predictions agreed very well with experimental data on the growth of keratinocyte megacolonies (Barrandon and Green, 1987). Model predictions also agreed well with experimentally measured proliferation rates of endothelial cells cultured in the presence of growth factors that stimulate cell motility.

We believe that the model described here has the potential to become a predictive tool because all of its parameters can be estimated from independent experimental data. The development of models with predictive ability is a necessary prerequisite for developing control strategies for biotechnological processes involving proliferation of anchorage-dependent, contact-inhibited cells.

This work was supported by a grant from the National Science Foundation (BCS-9216454).

REFERENCES

Alberts, B., D. Bray, J. Lewis, M. Raff, K. Roberts, and J. D. Watson. 1989. Molecular Biology of the Cell. Garland Publishing, New York.

Barrandon, Y., and H. Green. 1987. Cell migration is essential for sustained growth of keratinocyte colonies: the roles of transforming growth factor-α and epidermal growth factor. *Cell.* 50:1131–1137.

Cherry, R. S., and E. T. Papoutsakis. 1989. Modeling of contact-inhibited animal cell growth on flat surfaces and spheres. *Biotechnol. Bioeng.* 33:300–305.

Forestell, S. P., B. J. Milne, N. Kalogerakis, and L. A. Behie. 1992. A cellular automaton model for the growth of anchorage-dependent mammalian cells used in vaccine production. *Chem. Eng. Sci.* 47:2381–2386.

Frame, K. K., and W.-S. Hu. 1988. A model for density-dependent growth of anchorage-dependent mammalian cells. *Biotechnol. Bioeng.* 32: 1061–1066.

Gotlieb, A. I., W. Spector, M. K. K. Wong, and C. Lacey. 1984. In vitro reendothelization microfilament bundle reorganization in migrating porcine endothelial cells. *Arteriosclerosis.* 4:91–96.

Grotendorst, G. R., H. Seppa, H. K. Kleinman, and G. R. Martin. 1981. Attachment of smooth muscle cells to collagen and their migration toward platelet-derived growth factor. *Proc. Natl. Acad. Sci. USA.* 78:3669–3672.

Haudenschild, C. C., and S. M. Schwartz. 1979. Endothelial regeneration. II. Restitution of endothelial continuity. *Lab. Invest.* 41:407–418.

Hawboldt, K. A., N. Kalogerakis, and L. A. Behie. 1994. A cellular automaton model for microcarrier cultures. *Biotechnol. Bioeng.* 43: 90–100.

Ingber, D. E. 1990. Fibronectin controls capillary endothelial growth by modulating cell shape. *Proc. Natl. Acad. Sci. USA.* 87:3579–3583.

Klein-Soyer, C., A. Beretz, R. Millon-Collard, J. Abecassis, and J.-P. Cazenave. 1986. A simple in vitro model of mechanical injury of confluent cultured endothelial cells to study quantitatively the repair process. *Thromb. Haemost.* 56:232–235.

Lee, Y. 1994. Computer-assisted analysis of endothelial cell migration and proliferation. Ph.D. thesis. Rice University, Houston, TX.

Lee, Y., L. V. McIntire, and K. Zygourakis. 1994. Analysis of endothelial cell locomotion: differential effects of motility and contact inhibition. *Biotechnol. Bioeng.* 43:622–634.

Lim, J. H. F., and G. A. Davies. 1990. A stochastic model to simulate the growth of anchorage dependent cells on flat surfaces. *Biotechnol. Bioeng.* 36:547–562.

McNeil, P. L., L. Muthukrishnan, E. Warder, and P. A. D'Amore. 1989. Growth factors are released by mechanically wounded endothelial cells. *J. Cell Biol.* 109:811–822.

Noble, P. B., and M. D. Levine. 1986. Computer-Assisted Analysis of Cell Locomotion and Chemotaxis. CRC Press, Boca Raton, FL.

Reidy, M. A., and S. M. Schwartz. 1981. Endothelial regeneration. III. Time course of intimal changes after small defined injury to rat aortic endothelium. *Lab. Invest.* 44:301–308.

Ross, R. 1993. The pathogenesis of atherosclerosis: a perspective for the 1990s. *Nature.* 362:801–809.

Ross, R., and A. Vogel. 1978. The platelet-derived growth factor. *Cell.* 14:203–210.

Ruaan, R.-C., G.-J. Tsai, and G. T. Tsao. 1993. Monitoring and modeling density-dependent growth of anchorage-dependent cells. *Biotechnol. Bioeng.* 41:380–389.

Rupnick, M. A., C. L. Stokes, S. K. Williams, and D. A. Lauffenburger. 1988. Quantitative analysis of random motility of human microvessel endothelial cells using a linear under-agarose assay. *Lab. Invest.* 59: 363–372.

Sato, Y., and D. B. Rifkin. 1988. Autocrine activities of basic fibroblast growth factor: regulation of endothelial cell movement, plasminogen activator synthesis, and DNA synthesis. *J. Cell Biol.* 107: 1199–1205.

Schwartz, S. M., C. M. Gajdusek, M. A. Reidy, S. C. Selden III, and C. C. Haudenschild. 1980. Maintenance of integrity in aortic endothelium. *Fed. Proc.* 39:2618–2625.

Schwartz, S. M., C. M. Gajdusek, and S. C. Selden III. 1981. Vascular wall growth control: the role of the endothelium. *Arteriosclerosis.* 1:107–161.

Schwartz, S. M., C. C. Haudenschild, and E. M. Eddy. 1978. Endothelial regeneration. I. Quantitative analysis of initial stages of endothelial regeneration in rat aortic intima. *Lab. Invest.* 38:568–580.

Selden, S. C., III, and S. M. Schwartz. 1979. Cytochalasin B inhibition of endothelial proliferation at wound edges in vitro. *J. Cell Biol.* 81: 348–354.

Stokes, C. L., and D. A. Lauffenburger. 1991. Analysis of roles of microvessel endothelial cell random motility and chemotaxis in angiogenesis. *J. Theor. Biol.* 152:377–403.

Stokes, C. L., D. A. Lauffenburger, and S. K. Williams. 1991. Migration of individual microvessel endothelial cells: stochastic model and parameter measurement. *J. Cell Sci.* 99:419–430.

Tchuente, M. 1987. Computation on automata networks. *In* Automata Networks in Computer Science. Theory and applications. F. Fogelman-

Soulié, Y. Robert, and M. Tchuente, editors. Princeton University Press, Princeton, NJ. 101–129.

Thilo-Korner, D. G. S., and R. I. Freshney. 1983. The Endothelial Cell—A Pluripotent Control Cell of the Vessel Wall. Karger Publishers, Basel, Switzerland.

Wang, N., and D. E. Ingber. 1994. Control of cytoskeletal mechanics by extracellular matrix, cell shape and mechanical tension. *Biophys. J.* 66:2181–2189.

Zygourakis, K., R. Bizios, and P. Markenscoff. 1991a. Proliferation of anchorage-dependent contact-inhibited cells. I. Development of theoretical models based on cellular automata. *Biotechnol. Bioeng.* 38: 459–470.

Zygourakis, K., and P. Markenscoff. 1991. Parallel iterations and cellular automata models for simulating certain structural transformation. *In* Proceedings of the 1991 ACM Computer Science Conference.

Zygourakis, K., P. Markenscoff, and R. Bizios. 1991b. Proliferation of anchorage-dependent contact-inhibited cells. II. Experimental results and validation of the theoretical models. *Biotechnol. Bioeng.* 38: 471–479.